Short Papers

Improved Positioning Accuracy of the PA10-6CE Robot with Geometric and Flexibility Calibration

Chris Lightcap, Samuel Hamner, Tony Schmitz, and Scott Banks

***Abstract*—Accurate determination of robot geometric and flexibility parameters permits significant reduction of systematic errors and improved end-effector positioning accuracy. We apply a 30-parameter flexible geometric model to the Mitsubishi PA10-6CE robot and reduce mean/peak positional errors from 1.80/2.45 mm to 0.33/0.71 mm while loaded at 44 N.**

***Index Terms*—Geometric calibration, joint flexibility, Mitsubishi PA10-6CE, parameter identification.**

I. Introduction

Robot-assisted surgery and biomechanical testing are just some of the many fields that require accurate measurement and control of robotic manipulators. Although joint resolver measurements are highly precise and lead to excellent positional repeatability for consistent loading conditions, this high repeatability does not guarantee accurate positioning performance. Accurate knowledge of link geometries and joint flexibilities are necessary for error compensation. It is essential to have an effective calibration procedure to determine geometric and flexibility parameters of an assembled robot, since these quantities are specific to a given manipulator.

The Mitsubishi PA10-6CE is a six-degree-of-freedom manipulator equipped with AC servo motors and harmonic drive transmissions. The large gear ratio and compact design of the harmonic drive makes it ideal for many robotic applications. However, these transmissions are known to exhibit nonlinear flexibility and frictional losses, kinematic error, and resonance vibration, making it difficult to estimate the true end-effector position from joint position alone [1], [2]. In addition, geometric modeling errors, common to all robotic manipulators, further increase end-effector positioning error. Link lengths, twist angles, and joint offsets reported by the manufacturer are only accurate to manufacturing and assembly tolerances. Small errors in these Denavit–Hartenberg (DH) parameters can propagate to create significant errors in end-effector position [3]. A flexible robot model and an effective calibration procedure are required to characterize geometric uncertainties and joint flexibilities.

Many researchers have implemented least-squares or nonlinear optimization techniques to calibrate robotic manipulators. Taghirad et al. developed a model of harmonic drive stiffness through a controlled loading experiment [4]. Kennedy and Desai modeled the stiffness component of joint torque on a Mitsubishi PA10-6CE as a function of the applied load [5]. The inclusion of both geometric and nongeometric errors appears in [6] and [7], but the authors used a set of generalized error functions and did not identify physically meaningful parameters. A physical relationship is desirable for: 1) extrapolation of points outside the calibrated workspace and 2) a kinematic and dynamic model used in model-based control algorithms. Khalil and Besnard recently developed a nonlinear least-squares method to calculate physically meaningful geometric and flexibility parameters [8].

The contribution of this paper is the design and execution of a two-level nonlinear optimization algorithm for the calibration of geometric and flexibility parameters in a serial manipulator using measurements from a coordinate measuring machine (CMM). This method offers greater simplicity than that in [8] since it does not require the computation of the generalized Jacobian matrix. In addition, we performed a Monte Carlo simulation of positioning error based solely on joint resolver uncertainties, establishing the absolute best-case robot positioning accuracy. Finally, we assessed the fidelity of our model with an experimental comparison of robot positioning accuracy for a novel set of configurations and end-effector loads before and after the calibration procedure. The generalization of this method and its extension to other serial manipulators are also discussed.

This paper is organized into four sections. Section II outlines the experimental setup and procedure. Section III details the results from the our experiment and simulation. Section IV provides the observations and conclusions.

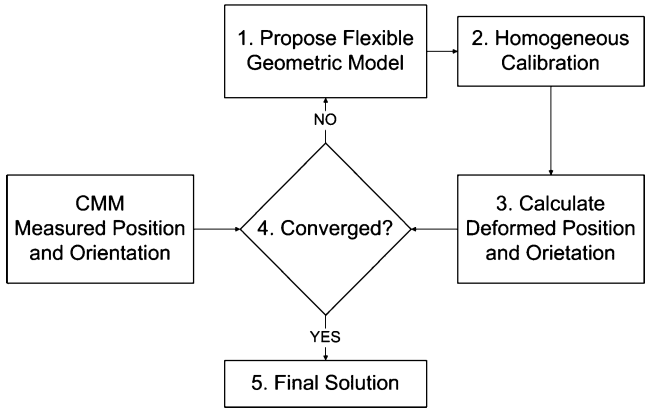

Fig. 1. Solution sequence for geometric and flexibility calibration.

II. Methods

A. Overview of Method

The computational resources needed for the solution of an optimization problem greatly increase with the addition of more design variables [9]. Hence, a multi level optimization method is employed to increase the speed of convergence (Fig. 1). First, a flexible geometric model is proposed by an outer level optimization. Next, an inner level optimization determines the best-fit homogeneous transformation between the CMM and robot coordinate systems. The inner level optimization converges quickly and reliably to a solution given a set of

Manuscript received June 6, 2007; revised October 12, 2007. This paper was recommended for publication by Associate Editor P. Rocco and Editor F. Park upon evaluation of the reviewers' comments. This work was supported by new faculty startup funds at the University of Florida.

C. Lightcap and T. Schmitz are with the Department of Mechanical and Aerospace Engineering, University of Florida, Gainesville, FL 32611 USA (e-mail: cal9@ufl.edu; tschmitz@ufl.edu).

S. Hamner was with the University of Florida, Gainesville, FL 32611 USA. He is now with the Department of Mechanical Engineering, Stanford University, Stanford, CA 94305 USA (e-mail: samner@stanford.edu).

S. Banks is with the Department of Mechanical and Aerospace Engineering and the Department of Orthopaedics and Rehabilitation, University of Florida, Gainesville, FL 32611 USA (e-mail: banks@ufl.edu).

Color versions of one or more of the figures in this paper are available online at http://ieeexplore.ieee.org.

Digital Object Identifier 10.1109/TRO.2007.914003

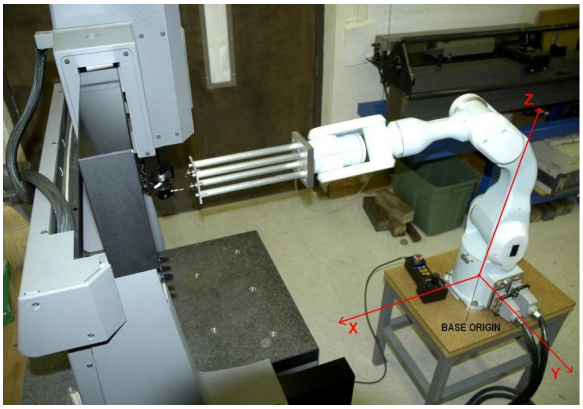

Fig. 2. Experimental setup of the PA10-6CE and CMM.

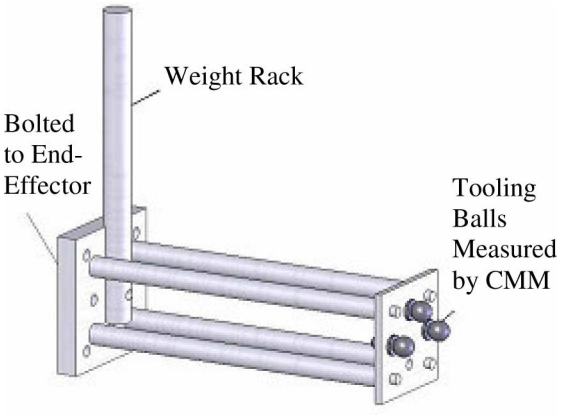

Fig. 3. Tooling-ball apparatus.

DH parameters and flexibility coefficients. It is, therefore unnecessary to burden the parent optimization algorithm with this subset of design variables. Next, using this model, the deflected position and orientation are computed from measured joint torques (via motor current) and compared to their respective CMM measurement. The final model is realized upon numerical convergence of this two-level optimization.

B. Experimental Setup and Procedure

A Mitsubishi PA10-6CE robot was positioned on a 0.6 m steel frame table so that its end-effector could span the entire workspace of a Brown and Sharpe, MicroVal PFX454 touch trigger probe CMM (Fig. 2). The CMM operates by probing the surface of a spherical tooling ball, and calculating the least-squares estimate of the centroid of the ball. A coordinate system was defined from the location of three tooling balls in the CMM workspace [10]. It had a calibrated measurement uncertainty of 12.1 μm over its full work volume.

To facilitate CMM measurement, a tooling-ball apparatus was constructed and mounted to the end-effector of the robot (Fig. 3). It comprised two parallel aluminum plates, separated by four 31 cm aluminum rods; the mass was 2.4 kg. The extension of tooling balls into the CMM workspace reduced the chance of impingement between the manipulator and the CMM table. The back-plate was attached to the end-effector of the robot, and the front-plate contained a set of three tooling balls. The transformation between the CMM coordinate system and a user-defined tooling ball coordinate system (BALL), ${}^{\mathrm{CMM}}_{\mathrm{BALL}}T$, was determined from measurements of the location of the tooling balls.

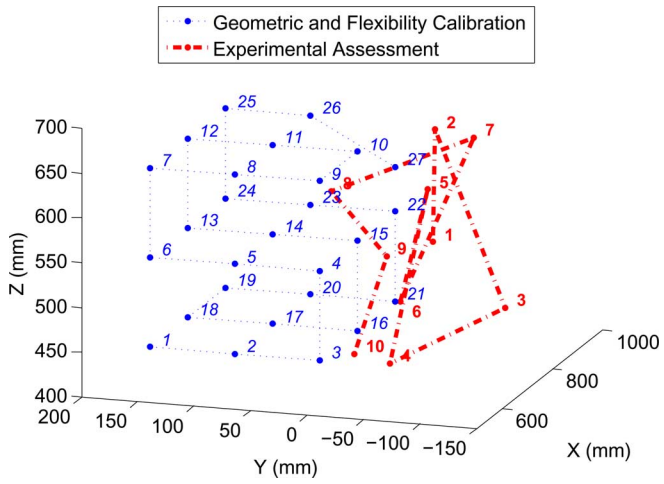

Fig. 4. Experimental test path.

The robot was commanded to move along a Cartesian pattern of uniformly distributed points in the CMM working volume (Fig. 4). At each static configuration, the CMM measured the position and orientation of the tooling ball coordinate system. The experiment was repeated ten times for each of three loading scenarios: {0, 22, and 44} N loads. External loads were provided by additional weights lowered onto the weight rack and secured with a set screw and shaft collar. The external load was transmitted through the end-effector of the robot, and therefore, did not create deflection in the rods (Fig. 3).

Maximum deflection of the apparatus from its own weight was 0.030 mm. The approximate touch force of the CMM was 0.2 N, creating a maximum deflection of less than 0.001 mm from contact. These deflections were negligible compared to the robot positioning error from uncertain geometric parameters and joint compliance.

C. Two-Level Geometric and Flexibility Calibration

A flexible geometric model was defined from a set of 30 design variables (Table I). It consisted of departures in link lengths, twist angles, joint offsets, and joint angles from their nominal values, represented by δa_i, $\delta\alpha_i$, δd_i, $\delta\beta_i$, and $\delta\theta_i$, respectively [10], and cubic spring coefficients for joints 2, 3, and 5, represented by $K_{\mathrm{lin},i}$ and $K_{\mathrm{cub},i}$ (joint 1 connects the base of the robot to the first link). The flexibility in the harmonic drive transmission was modeled with the torsional spring model

$$\tau = K_{\mathrm{lin}}\left(q_m - q\right) + K_{\mathrm{cub}}\left(q_m - q\right)^3, \tag{1}$$

where $q(t) \in \Re^n$ and $q_m(t) \in \Re^n$ denote the link and motor position, respectively, K_{lin} and $K_{\mathrm{cub}} \in \Re^{n\times n}$ are constant, diagonal, positive-definite matrices comprising the linear and cubic joint stiffness coefficients, respectively, and $\tau(t) \in \Re^n$ denotes the joint torque.

The departure in the Hayati parameter, labeled as $\delta\beta_2$, was substituted for δd_2 to eliminate the ill-conditioned transformation that exists between two parallel joints (i.e., joints 2 and 3) [11]. Nominal geometric parameters for the PA10-6CE geometry were taken from the manufacturer [12]. Joints 1, 4, and 6 were subject to negligible torques in the tested configurations, and as a result, stiffness coefficients were not estimated for them. Based on previous research with the PA10-6CE robot [8], link flexibility was not taken into account.

A two-level, Levenberg–Marquardt nonlinear least-squares optimization was implemented in MATLAB (Mathworks, Natick, MA) to solve for model parameters. The outer level optimization sought to find a flexible geometric model, consisting of 24 link parameters and six

TABLE I
DH PARAMETERS AND JOINT STIFFNESS COEFFICIENTS

Joint i	δa_i *(mm)*	$\delta\alpha_i$ *(rad)*	δd_i *(mm)*	$\delta\theta_i$ *(rad)*	$\delta\beta_i$ *(rad)*	$K_{lin,i}$ *(Nm/rad)*	$K_{cub,i}$ *(Nm/rad^3)*
1	0.33	-4.9 x 10^{-4}	0.09	-5.9 x 10^{-3}	n / a	∞	∞
2	–0.46	1.2 x 10^{-4}	n / a	–7.8 x 10^{-3}	-1.0 x 10^{-3}	1.98 x 10^{4}	3.35 x 10^{8}
3	1.09	-2.3 x 10^{-3}	1.26	2.9 x 10^{-3}	n / a	1.27 x 10^{4}	1.46 x 10^{8}
4	-0.48	2.1 x 10^{-4}	0.22	8.1 x 10^{-3}	n / a	∞	∞
5	-0.30	3.7 x 10^{-5}	0.10	-1.5 x 10^{-3}	n / a	2.56 x 10^{3}	3.84 x 10^{8}
6	-3.44	–7.1 x 10^{-4}	0.17	1.3 x 10^{-2}	n / a	∞	∞

stiffness coefficients, that satisfied

$$\vec{\mathrm{X}} = \arg\min_{\vec{\mathrm{X}}} f_{\text{outer}}, \tag{2}$$

where

$$f_{\text{outer}} = \frac{1}{r_{\max}^2}\sum_{i=1}^{N}(\vec{x}_i - \vec{x}_{i,m})^2 + \sum_{i=1}^{N}\left(\vec{\phi}_i - \vec{\phi}_{i,m}\right)^2 + \varepsilon\left[\sum\left(\frac{\delta a_i}{a_{i,\text{tol}}}\right)^2 + \sum\left(\frac{\delta\alpha_i}{\alpha_{i,\text{tol}}}\right)^2 + \sum\left(\frac{\delta d_i}{d_{i,\text{tol}}}\right)^2\right] + \varepsilon\left[\sum\left(\frac{\delta\beta_i}{\beta_{i,\text{tol}}}\right)^2 + \sum\left(\frac{\delta\theta_i}{\theta_{i,\text{tol}}}\right)^2\right]$$

and

$$\vec{\mathrm{X}} = [\,\delta a_i \quad \delta\alpha_i \quad \delta d_i \quad \delta\beta_i \quad \delta\theta_i \quad K_{lin,i} \quad K_{cub,i}\,],$$

where $\vec{x}_i$, $\vec{x}_{i,m}$, $\vec{\phi}_i$, and $\vec{\phi}_{i,m}$ represent the estimated and measured end-effector positions and orientations (parameterized as angular rotations), respectively, in the robot's coordinate system, and $N = 27$ is the number of robot configurations. The estimated location of the tool frame is a function of geometric and flexibility model contained in $\vec{\mathrm{X}}$. Position errors were normalized with respect to the total length of the manipulator, $r_{\max} = 1$ m; therefore, an orientation error of 1 rad corresponded to a distance error of one unit at full extension. The remaining terms in the cost function, which represent errors in estimated DH parameters, were normalized with respect to the approximate tolerances, $a_{i,\text{tol}} = 0.25$ mm, $\alpha_{i,\text{tol}} =$ 1e - 3 rad, $d_{i,\text{tol}} = 0.25$ mm, $\beta_{i,\text{tol}} =$ 1e - 3 rad, and $\theta_{i,\text{tol}} =$ 5e - 4 rad, and then, scaled with the weighting factor $\varepsilon =$ 1.6e - 4. Large ϵ increases the cost associated with DH parameter error, and therefore, forces the optimization algorithm to account for location errors without modifications to the geometric model. Instead, the optimization method will adjust torsional spring coefficients to minimize the given cost function.

The values for $\vec{x}_{i,m}$ and $\vec{\phi}_{i,m}$ were determined from the position and orientation of the end-effector in the robot coordinate system, as measured by the CMM,

$$\underset{\text{EE},M}{\overset{\text{BASE}}{}}T = \underset{\text{CMM}}{\overset{\text{BASE}}{}}T\,\underset{\text{BALL}}{\overset{\text{CMM}}{}}T\,\underset{\text{EE},M}{\overset{\text{BALL}}{}}T \tag{3}$$

where $\underset{\text{BALL}}{\overset{\text{CMM}}{}}T$ is the transformation between CMM and tooling ball coordinate systems, $\underset{\text{EE},M}{\overset{\text{BALL}}{}}T$ is the known constant transformation between end-effector and tooling ball coordinate systems, and $\underset{\text{CMM}}{\overset{\text{BASE}}{}}T$ is the transformation between robot and CMM coordinate systems. The transformation $\underset{\text{BALL}}{\overset{\text{CMM}}{}}T$ was calculated from the CMM measurement of the tooling balls, $\underset{\text{EE}}{\overset{\text{BALL}}{}}T$ was determined from a separate measurement of the tooling ball apparatus, and $\underset{\text{CMM}}{\overset{\text{BASE}}{}}T$ was computed from the inner-level optimization.

At each iteration in the outer level optimization, defined in (2), an inner level optimization was performed using the updated flexible geometric model. The second optimization algorithm searched for the six-robot coordinate system parameters that satisfied

$$\vec{\Psi} = \arg\min_{\vec{\Psi}} f_{\text{inner}}, \tag{4}$$

where

$$f_{\text{inner}} = \frac{1}{r_{\max}^2}\sum_{j=1}^{M}(\vec{x}_j - \vec{x}_{j,m})^2 + \sum_{j=1}^{M}(\vec{\phi}_j - \vec{\phi}_{j,m})^2,$$

and

$$\vec{\Psi} = [\,{}^{\text{base}}p_{\text{cmm\_}o} \quad \gamma_x \quad \gamma_y \quad \gamma_z\,],$$

where ${}^{\text{base}}\vec{p}_{\text{cmm\_}o}$ is the origin of the CMM coordinate system in the robot coordinate system, γ_x, γ_y, and γ_z are a set of body-fixed angular rotations describing the orientation of the CMM coordinate system with respect to the robot coordinate system, and $M = 8$ is the number of robot configurations. The measured location of the tool frame, obtained from (3), is a function of robot coordinate system parameters contained in $\vec{\Psi}$. The subscript *j* has been introduced to differentiate from configurations in the outer level (subscript *i*). The total kinematic model has 30 parameters, consisting of 24 link parameters and six robot coordinate system parameters, and is minimum, complete, and parametrically continuous (MCPC) [13]. Link parameters were determined through the outer optimization loop, while robot coordinate system parameters were determined in the inner optimization loop. The optimization was repeated with different initial guesses to mitigate the problem of finding local minima.

The initial seed for the inner-level optimization, provided in (4), was estimated from end-effector measurements along a straight line. The robot followed a linear path along its *x*- and *y*-axes allowing for least-squares best-fit approximations to ${}^{\text{CMM}}\vec{x}_{\text{BASE}}$ and ${}^{\text{CMM}}\vec{y}_{\text{BASE}}$. The *z*-axis and reformulated y-axis were determined from

$${}^{\text{CMM}}\vec{z}_{\text{BASE}} = {}^{\text{CMM}}\vec{x}_{\text{BASE}} \times {}^{\text{CMM}}\vec{y}_{\text{BASE}}, \tag{5}$$

and

$${}^{\text{CMM}}\vec{y}_{\text{BASE}} = {}^{\text{CMM}}\vec{z}_{\text{BASE}} \times {}^{\text{CMM}}\vec{x}_{\text{BASE}}. \tag{6}$$

The last step was taken to ensure orthogonality between all measured axes. The initial seed or Euler angle rotations was determined from the rotation matrix $\underset{\text{BASE}}{\overset{\text{CMM}}{}}R$ [10].

$$\underset{\text{BASE}}{\overset{\text{CMM}}{}}R = [\,{}^{\text{CMM}}\vec{x}_{\text{BASE}} \quad {}^{\text{CMM}}\vec{y}_{\text{BASE}} \quad {}^{\text{CMM}}\vec{z}_{\text{BASE}}\,] \tag{7}$$

D. Monte Carlo Simulation

Joint resolver uncertainties cannot be reduced through calibration, and therefore, they determine the lower bound for end-effector positioning uncertainties. A Monte Carlo simulation using the six joint positions as simulation variables was implemented to determine the

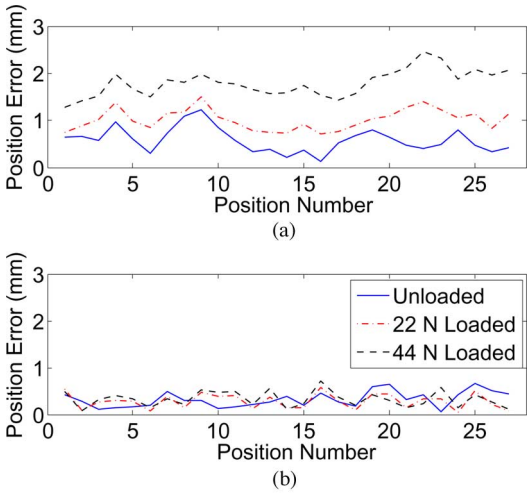

Fig. 5. Mean position error before and after calibration.

lower bound for robot position errors. For the PA10-6CE, the manufacturer reported a ± 0.64 arc min (0.011°) error in the angular position measurement of each link [14]. The probability distribution of each uncertain joint position was assumed to be Gaussian with a standard deviation equal to the reported bounds of that parameter. A forward kinematic analysis was performed for 100 000 cycles at each of the 200 uniformly selected end-effector positions in a given plane. The experiment was repeated for each cross-sectional plane located between $z = 400$ mm and $z = 700$ mm in 100 mm increments.

E. Experimental Assessment

The fidelity of the flexible geometric model was examined with a collection of ten points not included in the data used for model calibration (Fig. 4). The new set of data included configurations as far as 100 mm from the original control volume and loads up to 90 N, twice the original maximum load. The configuration order and loading order were selected arbitrarily. A comparison was made between the full model and a linear stiffness model ($K_{\text{cub}} = 0$).

III. Results

A. Monte Carlo Simulation

The Monte Carlo simulation determined a mean endpoint position error of 0.197 mm $\pm$ 0.096 mm in the xy-plane of $z = 500$ mm. Results from parallel planes at $z = 300$ mm and $z = 700$ mm deviated by less than 0.001 mm.

B. Geometric and Flexibility Calibration

The mean/peak values of position error prior to geometric and flexibility calibration were 0.58/1.22 mm, 1.02/1.50 mm, and 1.80/2.45 mm for the unloaded, 22 N loaded, and 44 N loaded cases, respectively (Fig. 5). The standard deviations of position error, within one configuration, did not exceed 0.014, 0.024, and 0.023 mm, for each loading case, respectively. After the optimization of robot geometry and joint stiffnesses, the mean/peak values of position error decreased to 0.32/0.66, 0.28/0.58 mm, and 0.33/0.71 mm, respectively. Mean orientation error, defined as the L_2- norm of the difference in the sequence of Euler angle rotations (xyz) between measurements, was reduced from 1.2°, 1.2°, and 1.1° to 0.05°, 0.04°, and 0.03°, in each of the three loading cases, respectively.

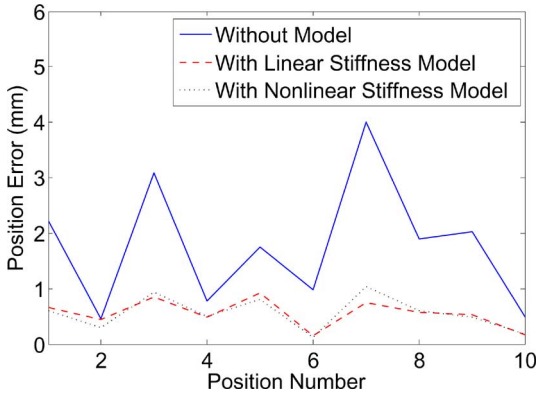

Fig. 6. End-effector position error at novel configurations and loads.

Linear joint stiffnesses identified by the two-level optimization were 1.98×10^4, 1.27×10^4, and 2.56×10^3 Nm/rad for joints 2, 3, and 5, respectively. The cubic joint stiffnesses were 3.35×10^7, $[1.46 \times 10^7,]$ and 3.83×10^7 Nm/rad^3, respectively.

C. Experimental Assessment

Mean positioning errors from uncalibrated configurations decreased from 1.77 to 0.55 mm with the linear stiffness model, and to 0.56 mm with the nonlinear stiffness model (Fig. 6). The peak value of position error decreased from 4 mm in the uncalibrated model to 0.92 and 1.04 mm with linear and nonlinear stiffness models, respectively. There was at least a 75% reduction in peak positioning error with both models. Mean orientation errors decreased from 2.4° to 1.2° with both models.

IV. Conclusion

The 30 parameter flexible geometric model has been demonstrated to improve static positioning accuracy for the PA10-6CE robot. End-effector positioning errors decreased substantially (Fig. 5), showing 50–80% reductions in mean position errors across all robot configurations. Measured positioning errors (0.3 mm) differed by less than 0.1 mm from their theoretical minimum determined from Monte Carlo simulation. DH parameters were all within reasonable manufacturing and assembly tolerances for the PA10–6CE. The large value for δa_6 is most likely from error in measuring the transformation between end-effector and tooling ball coordinate systems, and in assembling the tooling ball apparatus on the end-effector. The superior performance of the model while extrapolating outside the calibrated configurations is a good indication of its strength.

The linear stiffness model performed surprisingly well in the experimental assessment (Fig. 6). Nonlinearities that exist in harmonic drive transmissions are most prominent at small operating loads [1] and the joint torques in this experiment, for the most part, fall outside of this region. It may be worth considering a linear stiffness model given its simplicity and similar performance.

The method described in this paper can be generalized to any serial manipulator represented by DH parameters. In the case of a perfectly rigid-joint manipulator, stiffness parameters returned from the optimization would approach infinity.

Accuracy standards for robot-assisted surgery depend upon the application. Radiation therapy is one of the most demanding applications and some believe positioning errors greater than 0.5 mm increase patient risk [15]. Robotic applications in orthopaedic surgery typically seek to achieve positioning errors less than 1 mm or 1° for bone cutting [16]. It appears that these demanding requirements can be met by

the PA10-6CE utilizing the geometric and flexibility calibration method described here. We anticipate the combination of a detailed physical model, and its accompanying control design will provide an accurate measurement and control system suitable for demanding dynamic applications with the PA10-6CE robot arm.

ACKNOWLEDGMENT

The authors thank N. Mauntler for help in operating the CMM and J. D. Yamokoski for much appreciated suggestions on the calibration approach.

REFERENCES

[1] T. D. Tuttle, "Understanding and modeling the behavior of a harmonic drive gear transmission,". (1992). *MIT Artif. Intell. Lab.,* Cambridge, MA, Tech. Rep. 1365, 1992, 1992.
[2] N. Kircanski and A. A. Goldenberg, "An experimental study of nonlinear stiffness, hysteresis, and friction effects in robot joints with harmonic drives and torque sensors," *Int. J. Robot. Res.*, vol. 16, no. 2, pp. 214–239, 1997.
[3] R. P. Judd and A. B. Knasinski, "A technique to calibrate industrial robots with experimental verification," *IEEE Trans. Robot. Autom.*, vol. 6, no. 1, pp. 20–30, Feb. 1990.
[4] H. D. Taghirad, P. R. Belanger, and A. Helmy, "An experimental study on harmonic drives,". (1996). *International Submarine Engineering Ltd., McGill Univ. Center for Intell. Mach, Tech. Rep., 1996*. 1996.
[5] C. W. Kennedy and J. P. Desai, "Modeling and Control of the Mitsubishi PA10 Robot Arm Harmonic Drive System," *IEEE/ASME Trans. Mechatronics*, vol. 10, no. 3, pp. 263–274, Jun. 2005.
[6] J. H. Jang, S. H. Kim, and Y. K. Kwak, "Calibration of geometric and non-geometric errors of an industrial robot," *Robotica*, vol. 19, pp. 311–321, 2001.
[7] M. A. Meggiolaro, S. Dubowsky, and C. Mavroidis, "Geometric and elastic error calibration of a high accuracy patient positioning system," *Mechanism Mach. Theory*, vol. 40, pp. 415–427, 2005.
[8] W. Khalil and S. Besnard, "Geometric calibration of robots with flexible joints and links," *J. Intell. Robotic Syst.*, vol. 34, pp. 357–379, 2002.
[9] R. T. Haftka and Z. Gurdal, *Elements of Structural Optimization*, 3rd ed. Dordrecht, The Netherlands: Kluwer Academic, 1992, pp. 387–414.
[10] C. D. Crane III and J. Duffy, *Kinematic Analysis of Robot Manipulators*. Cambridge, U.K.: Cambridge Univ. Press, 1998, ch. 2.
[11] S. A. Hayati, "Robot arm geometric link calibration," in *Proc. 22nd IEEE Conf. Decis. Control*, 1983, pp. 1477–1483.
[12] *Instruction Manual for Installation, Maintenance, and Safety*, Mitsubishi Heavy Industries, Tokyo, Japan, 2003.
[13] B. W. Mooring, Z. S. Roth, and M. R. Driels, *Fundamentals of Manipulator Calibration*. Hoboken, NJ: Wiley, 1991.
[14] Variable Resolution, *Monolithic Resolver-to-Digital Converters*. Norwood, MA: Analog Devices, 1998.
[15] C. Mavroidis, J. Flanz, S. Dubowsky, P. Drouet, and M. Goitein, "High performance medical robot requirements and accuracy analysis," *Robot. Comput. Integr. Manuf.*, vol. 14, no. 5–6, pp. 329–338, 1998.
[16] R. D. Howe and Y. Matsuoka, "Robotics for surgery," *Annu. Rev. Biomed. Eng.*, vol. 1, pp. 211–240, 1999.

Discretization of a Continuous Curve

Sean B. Andersson

***Abstract*—We consider the problem of approximating a finite-length continuous curve by a piecewise linear one whose segments are assumed to be connected by 2 DOF joints. We solve the problem under the assumption that the endpoints of the line segments lie on the continuous curve. Analytical expressions for the relative orientations of each pair of line segments as a function of a single rotational DOF are found. This angle can be chosen arbitrarily or used to optimize a secondary task. The motivating application for this paper is the control of a snake-like robot using gaits designed from shape primitives.**

***Index Terms*—Kinematics, snake-like robot.**

I. INTRODUCTION

In this paper, we consider the problem of approximating a continuous, finite-length 3-D curve with a piecewise linear one. The discrete curve consists of a sequence of blocks, each of which is connected to a line segment at its center by a revolute joint. Each internal block is connected to two line segments, and we assume that the joint axes are orthogonal, yielding a 2 DOF joint. We simplify the problem by assuming that the center of each block lies on the continuous curve. The location of these points along the curve to be approximated are found numerically using a bisection search method. Given these locations, we derive expressions for the joint angles as a function of a single DOF, namely a rotation of the first segment around the axis defined by its endpoints. This rotation can be either chosen arbitrarily or used to optimize some secondary task. The algorithm for the calculation of the joint angles is $O(n)$ in complexity where n is the number of line segments in the discrete curve.

The motivation for this research lies in the control of snake-like (or hyperredundant) mobile robots. This class of robot, pioneered by the active-cord mechanism of Hirose [1], provides a flexibility that is difficult or impossible to achieve with other locomotion modalities. The algorithm presented here can also be used for the control of a hyperredundant manipulator. These manipulators have the capability to perform unconventional tasks such as pipeline inspection, minimally invasive surgery [2], and whole-arm manipulation [3]. The very flexibility of such systems make them difficult to control. Many redundancy resolution schemes utilize some form of inverse of the Jacobian, often coupled with numerical optimization [4]–[6]. However, due to the very large number of DOFs for hyperredundant robots, the computational burden of these techniques is generally prohibitive.

An alternative approach is to perform path planning for the robot using a continuous-curve approximation. This is coupled with a fitting process for determining the joint angles such that the robot takes on the desired shape [7]–[11] or by determining the sequence of joint angles such that the robot extends outward along the path [12], [13]. In many cases, the fitting is achieved through numerical minimization of a distance function between the continuous curve and the robot. In [14], the authors avoid the need to directly solve the inverse kinematics

Manuscript received June 1, 2007; revised November 7, 2007. This paper was recommended for publication by Associate Editor S. Ma and Editor F. park upon evaluation of the reviewers' comments. This work was supported in part by the Defense Advanced Research Projects Agency (DARPA) under a Charles S. Draper Laboratory Prime DL-H-551034.

The author is with the Department of Aerospace and Mechanical Engineering, Boston University, Boston, MA 02215 USA (e-mail: sanderss@bu.edu).

Color versions of one or more of the figures in this paper are available online at http://ieeexplore.ieee.org.
Digital Object Identifier 10.1109/TRO.2008.917000